Journal of Electroceramics 3:1, 25–36, 1999

The Structure and Defect Chemistry of Non-Stoichiometric Nickel Molybdates

DORON LEVIN & JACKIE Y. YING*

Department of Chemical Engineering, Massachusetts Institute of Technology, Cambridge, MA 02139

Submitted March 2, 1998; Revised September 23, 1998; Accepted December 11, 1998

Abstract. A series of materials represented by the formula $Ni_{1+\delta}Mo_{1-\delta/3}O_4$, where $-1/5 \leq \delta \leq 1/3$, were prepared by calcination of layered ammonium nickel molybdates having a general formula $(NH_4)H_{2x}Ni_{3-x}O(OH)(MoO_4)_2$, where $0 \leq x \leq 3/2$. Phase determination using high temperature X-ray diffraction studies showed that the variable stoichiometry of the precursor phase that allowed for Ni/Mo ratios between 0.75 and 1.5 led to the formation of a single phase of the form $Ni_{1+\delta}Mo_{1-\delta/3}O_4$ following calcination. AC impedance spectroscopy was used to investigate the electronic conductivity of the materials. The defect chemistry of these ternary ionic materials was modeled to correlate the electronic conductivity with the structure.

Keywords: nickel molybdate, non-stoichiometry, defect structure, and electronic conductivity

Introduction

A fundamental understanding of the electronic nature of semiconducting catalysis is one area of research awaiting further exploitation. Research in this field seeks to answer many interesting questions on how the electronic properties of the catalyst surface itself affects the catalytic reactions taking place thereon. A fundamental understanding of the ability of a catalyst surface to interact with adsorbed gas molecules through the transfer of electron density will assist in the development of new catalysts having desired electronic properties. The electronic nature of a catalyst surface will influence the stability and reactivity of adsorbed species, and knowledge thereof is necessary to help explain many types of reactions that involve electron transfer from the catalyst to the reacting species.

Oxidation reactions, both combustion and partial oxidation reactions, make up a large percentage of the industrially important catalytic reactions currently used. The selective oxidative dehydrogenation (ODH) of lower alkanes into alkenes is a challenging problem in heterogeneous catalysis as the high bond energy of the primary C—H bond makes alkanes less reactive than the dehydrogenated alkenes. Transition metal molybdates are well known to be catalytically active for partial oxidation reactions, particularly for the selective oxidations of lower alkanes [1]. Of the transition metal molybdates, those based on nickel, and in particular the stoichiometric $NiMoO_4$, have attracted the greatest interest [2–5]. $NiMoO_4$ presents two polymorphic phases at atmospheric pressure: a low-temperature α phase, and a high-temperature β phase [2,4,6]. The β phase undergoes a transformation to the α phase when cooled below 180 °C [6]. Both phases are monoclinic with space group C2/*m*. These phases differ primarily in the coordination of molybdenum which is distorted octahedral in the α phase and distorted tetrahedral in the β phase. The β phase has been shown to be almost twice more selective in propene formation than the α phase for comparable conversion at the same temperature [2]. Prior research efforts into the catalytic properties of these phases have used a β phase prepared by high-temperature (700 °C) calcination of the α phase followed by cooling to reaction temperatures well above the $\beta \rightarrow \alpha$ transformation temperature. A

*To whom correspondence should be addressed.

similar phase dependence of selectivity has been noted for oxidative dehydrogenation of butane, with the β phase being approximately three times more selective in butene formation than the α phase [7]. The reason for the difference in selectivities is unknown, and a full understanding of the structure and properties of these materials is required to explain this difference.

A series of non-stoichiometric nickel molybdates of the form $Ni_{1+\delta}Mo_{1-\delta/3}O_4$, where $-1/5 \leq \delta \leq 1/3$, have been shown to produce higher propene yields than a stoichiometric $NiMoO_4$ [8]. Conversion of propane in an oxygen environment has been found to increase with decreasing Ni/Mo ratios [8]. The aim of this paper is to show that characterization of these catalysts suggests that they are essentially identical physically, leading to the conclusion that differences in their catalytic behavior could arise from differences in their electronic properties. An understanding of the structure and properties of this class of molybdates was therefore necessary to explain their catalytic behavior.

Experimental

1. Material Synthesis

The non-stoichiometric nickel molybdates were synthesized by calcination of layered ammonium nickel molybdate precursors having a general formula $(NH_4)H_{2x}Ni_{3-x}O(OH)(MoO_4)_2$, where $0 \leq x \leq 3/2$. These precursors are members of a class of layered transition metal molybdates, termed LTM, that have a general formula $(NH_4)H_{2x}A_{3-x}O(OH)(MoO_4)_2$, where A is a transition metal, or combination of transition metals, and $0 \leq x \leq 3/2$ [9]. The Ni-LTM precursors were synthesized by precipitation from aqueous solution [10]. Ammonium heptamolybdate (Aldrich Chemical Co.) and nickel nitrate (99.999% purity, Aldrich Chemical Co.) were used to prepare precursors for a series of non-stoichiometric nickel molybdates of the form $Ni_{1+\delta}Mo_{1-\delta/3}O_4$ where $-1/5 \leq \delta \leq 1/3$, as shown in Table 1. All chemicals used were of the highest obtainable quality to minimize impurity incorporation in the materials.

The typical synthesis of a layered nickel molybdate precursor is as follows. Ammonium heptamolybdate $((NH_4)_6Mo_7O_{24} \cdot 4H_2O)$ and nickel nitrate $(Ni(NO_3)_2 \cdot 6H_2O)$ were used to prepare a solution containing Ni and Mo in the desired molar ratio. The addition of concentrated ammonium hydroxide (28.8% NH_3) precipitated a green solid that dissolved in an excess of ammonia to give a deep blue solution. This solution was heated with constant stirring for 4 h, leading to the formation of a pale green precipitate. The products were isolated by vacuum filtration, washed with deionized water, and dried overnight at 110 °C and atmospheric pressure. The precursors were fine green powders.

The non-stoichiometric nickel molybdates were prepared by calcination of these Ni-LTM precursors. Calcination was typically carried out *in situ* at a temperature of 550 °C. Thermogravimetric analysis on a Perkin Elmer Series 7 TGA showed that the weight loss was independent of the calcination atmosphere. The weight loss as a function of temperature is shown in Fig. 1 for the preparation of a $NiMoO_4$ phase. The precursor phase decomposes with the loss of water and ammonia from the structure. Analysis of the TGA off-gas by mass spectroscopy showed that at temperatures below 300 °C, the weight loss can be attributed to the removal of water from the structure. This water is predominately surface adsorbed water since analysis of a sample washed in acetone showed a 50% reduction in the weight loss below 300 °C. Thermal analysis by differential scanning calorimetry on a Perkin Elmer Series 7 DSC showed that the transformation from the precursor to the $Ni_{1+\delta}Mo_{1-\delta/3}O_4$ phase occurred

Table 1. Catalysts derived from $(NH_4)H_{2x}Ni_{3-x}O(OH)(MoO_4)_2$ precursors

x	Ni/Mo ratio	Precursor formula	Catalyst formula	δ
0.0	1.5	$(NH_4)Ni_3O(OH)(MoO_4)_2$	$Ni_{1.333}Mo_{0.889}O_4$	0.333
0.5	1.25	$(NH_4)Ni_{2.5}(OH)_2(MoO_4)_2$	$Ni_{1.176}Mo_{0.941}O_4$	0.176
1.0	1.0	$(NH_4)HNi_2(OH)_2(MoO_4)_2$	$NiMoO_4$	0.000
1.25	0.875	$(NH_4)H_{1.5}Ni_{1.75}(OH)_2(MoO_4)_2$	$Ni_{0.903}Mo_{1.032}O_4$	−0.097
1.5	0.75	$(NH_4)H_2Ni_{1.5}(OH)_2(MoO_4)_2$	$Ni_{0.80}Mo_{1.067}O_4$	−0.200

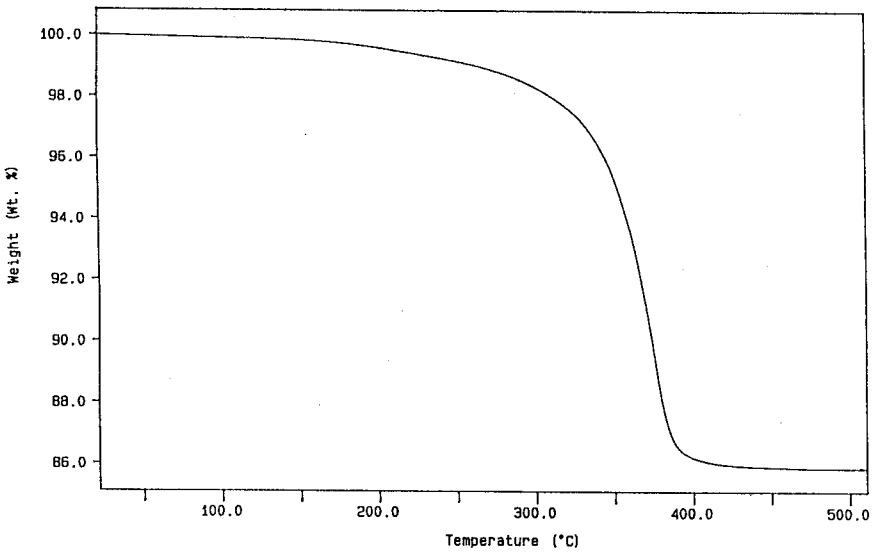

Fig. 1. Weight loss as a function of temperature for the $(NH_4)HNi_2(OH)_2(MoO_4)_2 \rightarrow NiMoO_4$ transformation.

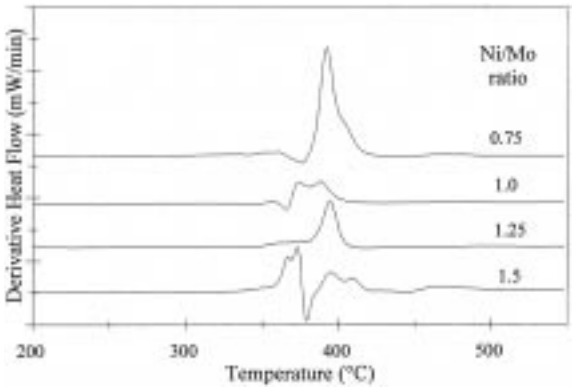

Fig. 2. Derivative of heat flow (mW/min) for calcination of Ni-LTM phases.

over a temperature range from 350 °C to 425 °C, as shown in Fig. 2. These thermal analysis studies showed that at a temperature of 550 °C at which the non-stoichiometric nickel molybdate phase was prepared and characterized, the transformation from the precursor was complete.

2. *Characterization of the Nickel Molybdates Prepared by Calcination*

2.1. X-Ray Diffraction (XRD). Room-temperature XRD patterns of calcined nickel molybdates are not true reflections of the actual phase present at higher temperatures due to a $\beta \rightarrow \alpha$ phase transformation that occurs on cooling [6]. To fully characterize this phase, high-temperature powder XRD patterns were collected with CuKα radiation using a Rigaku RU200 rotating anode $\theta/2\theta$ diffractometer equipped with a Rigaku 2311B high-temperature attachment. The high-temperature attachment was controlled using a Rigaku PTC-10C programmable temperature controller. Due to the vertical alignment of the sample holder, the Ni-LTM precursors were pressed into pellets of 8 mm diameter for analysis. The pellets were mounted to the vertical sample holder and held in place by two 0.008″ platinum wires that ran across the upper and lower portion of the pellet face. For an analysis, the sample was ramped to 550 °C at a rate of 20 °C/min in air, and then held isothermally for 30 min before collecting a scan. Following this scan, the sample was ramped to 700 °C at a rate of 20 °C/min and held there for 30 min before a scan was collected.

2.2. Diffuse reflectance infrared Fourier-transform (DRIFT) spectroscopy. The nature of the phase present under typical ODH reaction conditions was further characterized by collecting infrared spectra of the materials following *in situ* calcination of the precursors in a Harrick Scientific DRA3-HTC high-temperature diffuse reflectance accessory. This accessory enabled a controlled atmosphere to be maintained around the sample under investigation. Infrared spectra were collected using a BioRad FTS-

60A spectrometer. The Ni-LTM precursors, prepared as a 10 wt% mixture with KBr, were calcined with high-purity He flowing through the cell at a rate of 30 ml/min. The DRIFT spectra were collected at a sample temperature of 550 °C.

2.3. Electrical conductivity. The electrical conductivity of the series of non-stoichiometric nickel molybdates listed in Table 1 was characterized by 2-probe ac impedance spectroscopy. Initial attempts to characterize the electrical conductivity using 4-probe dc measurements were unsuccessful due to the mixed ionic/electronic nature of the material. On application of an applied voltage, the current decayed over time. The reason for this phenomenon is the movement of vacancies and anions under the application of an external electric field that sets up an internal chemical potential by the separation of charged species, counteracting the external applied field. To overcome this complication, impedance spectroscopy, an ac measurement technique, was used to determine the conductivity of the materials.

2.3.1. Experimental setup for impedance measurements. To measure ac conductivity, a tube furnace was set up in which a sample could be held in a controlled atmosphere, thereby allowing measurements at varying temperatures and oxygen partial pressures. The sample temperature was monitored by a Pt/Rh thermocouple located at the same axial position in the furnace tube as the sample. Radial temperature gradients within the 1″ O.D. alumina furnace tube were assumed to be negligible. To control the atmosphere within the tube furnace, a series of MKS Mass Flow Controllers were used to provide O_2/Ar gas mixtures over a range of O_2 concentrations from 0.25% to 100%. For the ac measurements, a Solartron 1260 Impedance/Gain-Phase Analyzer was used. This unit has a built in synthesizer that produces a stable voltage or current drive over the frequency range of 10 μHz to 32 MHz. The reported accuracy of the 1260 unit for impedance measurements of resistance is 0.1% to $10^5\Omega$, 1% to $10^7\Omega$, and 10% to $10^8\Omega$.

A key feature of this experimental setup involved the design of a suitable electrode system that would provide contacts of good electrical and mechanical quality. The materials under investigation introduced certain limitations on the type of electrode that could be used. Typically, conductivity studies are performed on ceramic materials that can be sintered at high temperatures to provide strong, dense pellets that can be machined and subjected to other forms of mechanical and thermal treatments. This allows for specific bonds between the material under investigation and the electrode material to be generated by high-energy processes including sputtering, soldering, and furnace-cured paints or pastes. The nickel molybdates under investigation though, do not allow for any type of thermal treatment due to the metastability of the β-phase at elevated temperatures that cause them to revert to the α phase on cooling to room temperature. The $\beta \rightarrow \alpha$ phase transformation involves a volume change of about 6% that could lead to the separation of an electrode, assuming that an electrode could be applied at elevated temperatures. It would be preferable to have an electroding technique that would allow for a good contact to be maintained through an LTM$\rightarrow\beta$-phase transformation. This led to the use of a mechanical bond formed by wedging a platinum electrode material to the face of a pellet of the specimen under investigation. It was also desirable to have a setup in which the position of the electrodes was fixed, and therefore would not change as various different samples were investigated. To accomplish these goals, a sample holder, shown schematically in Fig. 3, was designed and custom machined from 98% Al_2O_3. This sample holder was designed to reduce variability in the electrode/sample interface between various samples being measured. The electrode positions were fixed by the sample holder, and therefore did not depend on the sample itself. Platinum was used as the electrode material, with the Pt leads being shielded by a 4-bore alumina tube. When performing 2-probe ac conductivity measurements, electrodes 1 and 3 were coupled together, as were electrodes 2 and 4.

2.3.2. Impedance measurements. The electrical conductivity was measured on samples that had been pressed into cylindrical pellets under a pressure of 2300 kg/cm^2. The initial weight of the pellet was 150 mg. The pellet diameter was 10 mm, and the thickness of the LTM pellet was typically 0.93 mm. After calcination and the conclusion of the experiment, the pellet thickness was redetermined to allow for calculation of the electrical conductivity. The pellet thickness of the nickel molybdate phase was typically 0.86 mm.

Control of the Solartron 1260 Impedance/Gain-

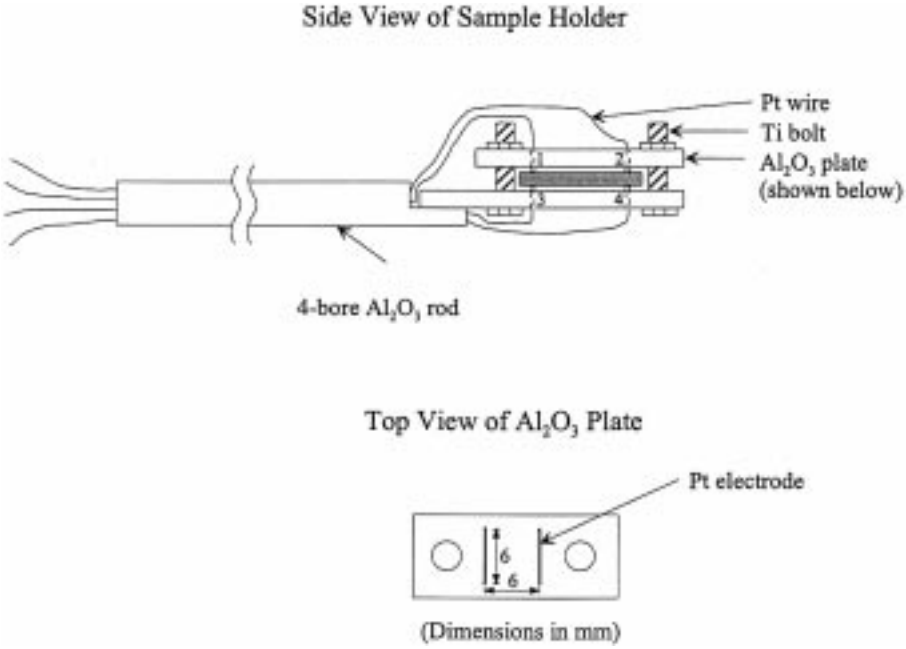

Fig. 3. Schematic of sample holder for electrical conductivity measurements.

Phase Analyzer and data collection of the ac impedance measurements occurred over a GPIB computer interface using Z-60/Z-View for Windows software (Scribner Associates, Inc.). Measurements were collected by controlling the current at 3 mA and sweeping the frequency from 5 MHz down to 1 Hz in logarithmic steps of 10 per decade. Impedance measurements were performed over a temperature range of 630 °C to 550 °C. The resistance of the samples was too high to allow for measurements to be taken at temperatures below 550 °C. Measurements were performed by either holding the temperature constant at 575 °C and varying the O_2 partial pressure from 0.25 kPa to 50 kPa, or by holding the O_2 partial pressure constant and varying the temperature. Before taking any measurements, pellets of the LTM precursor were calcined in 0.25 kPa of O_2 at 700 °C for 1 h, followed by calcination at 575 °C for 12 h. This pretreatment was necessary to burn off any hexadecanoic acid used as a lubricant on the pellet die, and to ensure that no shrinkage of the pellet occurred during data collection at the lower temperatures. In a series of experiments, the P_{O_2} would be set and three measurements would be taken at each temperature set point, starting at 630 °C. After each trio of measurements, the temperature would be decreased by 12–15 °C intervals to 550 °C. After the last datum was collected at 550 °C, the P_{O_2} would be raised, the temperature returned to 630 °C, and the measurement series repeated. Measurements were always collected on the cooling cycle for each P_{O_2} value. The sample was allowed to equilibrate for at least 30 min before a measurement was performed.

All the experimental data collected in the study on non-stoichiometric nickel molybdates were in the form of single arcs, centered below the axis. The data were therefore fitted to an equivalent RC circuit consisting of a single resistor and capacitor in parallel. From the fitting parameters, the resistivity (R) was determined, thereby enabling calculation of the electrical conductivity.

Results and Discussion

1. Phase Determination of Non-Stoichiometric Nickel Molybdates

It was expected that the phase resulting from calcination of the ammonium nickel molybdate precursor, $(NH_4)H_{2x}Ni_{3-x}O(OH)(MoO_4)_2$ would be a form of $NiMoO_4$. Two questions, however, needed to be addressed: (i) which phase of $NiMoO_4$ existed under ODH reaction conditions, and (ii) given the

non-stoichiometry of the precursor phase that allowed for Ni/Mo ratios between 0.75 and 1.5, was a single phase of the form $Ni_{1+\delta}Mo_{1-\delta/3}O_4$ produced on calcination?

Besides the LTM precursor that would yield a stoichiometric $NiMoO_4$, precursors having a Ni/Mo ratio of 0.75 and 1.5 were chosen for the high-temperature X-ray diffraction studies as they represent the bounds on the Ni/Mo ratio set by the crystal structure of the layered ammonium nickel molybdate. The $(NH_4)H_{2x}Ni_{3-x}O(OH)(MoO_4)_2$ precursor has an upper bound on the Ni/Mo ratio that is set by full occupancy of the Ni site. The lower bound on the Ni/Mo ratio is set by the inability of the LTM structure to accommodate further additional protons required for charge balancing as the occupancy of the Ni site is reduced to its minimum value of 1/2. The XRD patterns of the phases present at 550 °C resulting from *in situ* calcination of these three precursors are shown in Fig. 4. In this figure, two strong peaks at approximately 39° and 46° 2θ have been removed—these peaks correspond to platinum (PDF # 4-0802) and resulted from the presence of two 0.008″ platinum wires that ran across the face of the pellet to attach it to the vertical sample holder. This figure clearly shows all three phases to be the same, with no additional phases arising as the Ni content is increased. By comparing the XRD patterns with that of α-$NiMoO_4$ (PDF # 33-0948), it was concluded that the phase at 550 °C was not the α phase.

To definitively determine that the phase represented by the XRD patterns shown in Fig. 4 is indeed that of β-$NiMoO_4$, a powder pattern for β-$NiMoO_4$ was simulated using GSAS [11]. It is known that

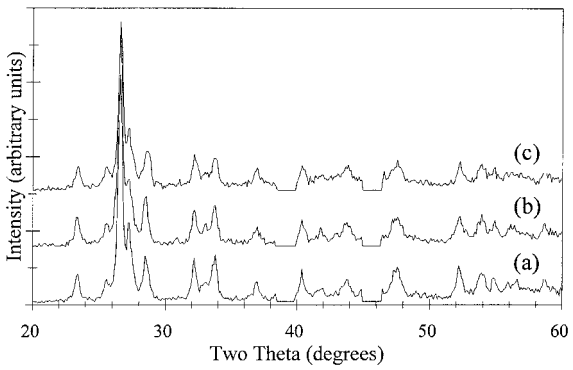

Fig. 4. XRD patterns collected at 550 °C following *in situ* calcination of the Ni-LTM precursors with a Ni/Mo ratio of (a) 0.75, (b) 1.0, and (c) 1.5.

Table 2. Structure Model for β-$NiMoO_4$

Atom	Wykoff	*x*	*y*	*z*
Ni (1)	4(h)	0	0.183	1/2
Ni (2)	4(i)	0.7953	0	0.1387
Mo (1)	4(g)	0	0.2516	0
Mo (2)	4(i)	0.2707	0	0.4050
O (1A)	4(i)	0.3587	1/2	0.4635
O (1B)	4(i)	0.2029	0	0.1534
O (2)	8(j)	0.1369	0.3548	0.1083
O (3)	8(j)	0.4584	0.3455	0.1904
O(4)	8(j)	0.3645	0.1504	0.4698

β-$NiMoO_4$ is isostructural to α-$MnMoO_4$, the structure of which has been previously determined [12]. Starting with the structure of α-$MnMoO_4$, the structure of β-$NiMoO_4$ could be modeled by replacing Mn with Ni on the 4(h) and 4(i) crystallographic positions, as detailed in Table 2. Cell dimensions of $a = 10.13$ Å, $b = 9.28$ Å, $c = 7.02$ Å, and $\beta = 107.2°$ were used [13]. Peak broadening was simulated using a multi-term Simpson's rule integration of the pseudo-Voigt function [14], as implemented in GSAS. Gaussian profile coefficients of $U = 200$, $V = -100$, $W = 20$, Lorentzian coefficients of $X = 1$, $Y = 35$, and an asymmetry correction factor of 3 were used. These values represent a rounded average of profile functions used to fit powder X-ray data of the precursors assumed to have a similar particle size to the calcined powders. The simulated powder pattern for β-$NiMoO_4$ is shown in Fig. 5. Comparison of the experimental XRD patterns shown in Fig. 4 to the simulated pattern definitively confirms that the phase present at 550 °C following calcination of the

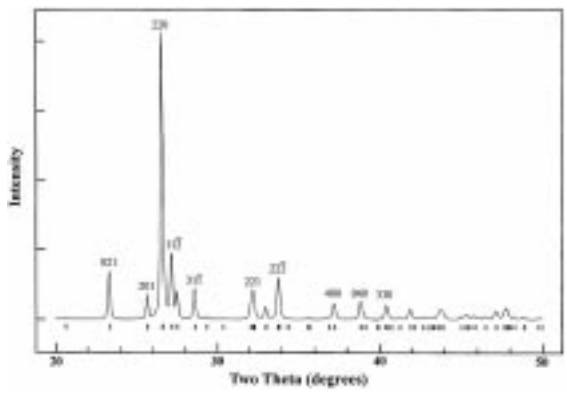

Fig. 5. Simulated diffraction pattern of β-$NiMoO_4$. The set of short vertical bars below the pattern indicate the position of possible Bragg reflections.

$(NH_4)H_{2x}Ni_{3-x}O(OH)(MoO_4)_2$ $(0 \leq x \leq 3/2)$ precursors is β-nickel molybdate.

The high-temperature diffraction studies also clearly show that no NiO exists as a secondary phase. Previous studies on the stability of β-$NiMoO_4$ have assumed that NiO exists as a secondary phase due to the presence of a diffraction peak at $\sim 37^\circ$ 2θ with CuKα radiation [6]. Nickel oxide does have a Bragg reflection at 37.2°, in addition to reflections at 43.3° and 62.9°, but the presence of a peak at 37.2° cannot be used to confirm the presence of NiO since β-$NiMoO_4$ has a (400) reflection at 37.1°, as shown in Fig. 5. In addition, the peak at 37° in Fig. 4(a) for the phase with a Ni/Mo ratio of 0.75 would not be present if this peak was due to the presence of ''excess'' Ni as NiO. The high-temperature XRD studies of these materials covering a Ni/Mo ratio of 0.75 to 1.5 also showed that no diffraction peaks arose at 43.3° that would indicate the presence of NiO.

The presence of a pure phase of β-$Ni_{1+\delta}Mo_{1-\delta/3}O_4$ at a temperature of 550 °C results from the use of the $(NH_4)H_{2x}Ni_{3-x}O(OH)(MoO_4)_2$ precursor. If this β-$Ni_{1+\delta}Mo_{1-\delta/3}O_4$ is subsequently allowed to cool back down to room temperature, the material undergoes a $\beta \rightarrow \alpha$ phase transformation. Reheating of this α phase to 550 °C does not, however, produce the β phase, as shown in Fig. 6. In accordance with results published in the literature [2], a temperature of at least 700 °C was required to transform the α phase back to the β phase. Since the surface area of the catalyst decreases with an increase in the calcination temperature, the production of a β-nickel molybdate from the α phase is undesirable. The direct conversion to β-nickel molybdate at a relatively low temperature of 550 °C made possible with the use of the Ni-LTM precursor offers an attractive route for catalyst preparation.

The normal stretching modes of the molybdate ions were expected to occur in the region 700–1000 cm^{-1} [15]. Figure 7 shows the DRIFT spectra of the phases present at 550 °C resulting from *in situ* calcination of the three precursors having a Ni/Mo ratio of 0.75, 1, and 1.5. This figure shows that all three materials, representing the full range of Ni/Mo ratios possible, have identical stretching modes. The four bands present between 700 and 1000 cm^{-1} suggest that the coordination around the molybdenum ions is tetrahedral. The bands centered at 945 cm^{-1} and 709 cm^{-1} can be assigned to a symmetric stretching vibration and an asymmetric stretch, respectively [15]. The bands centered at 872 cm^{-1} and 799 cm^{-1} can be assigned to ν_1 and ν_3 modes, respectively, noting that the intensity of ν_3 is slightly greater than that of ν_1, as is typical with oxometallates [15]. These

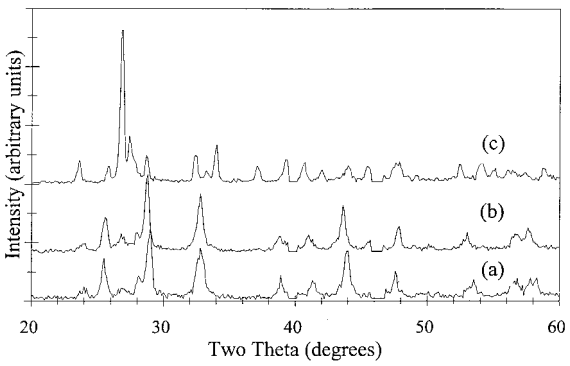

Fig. 6. XRD patterns of (a) α-$NiMoO_4$ derived by precalcining Ni-LTM at 550 °C, scanned at 25 °C, (b) material in (a) reheated in situ to 550 °C, and (c) material in (a) heated in situ to 700 °C.

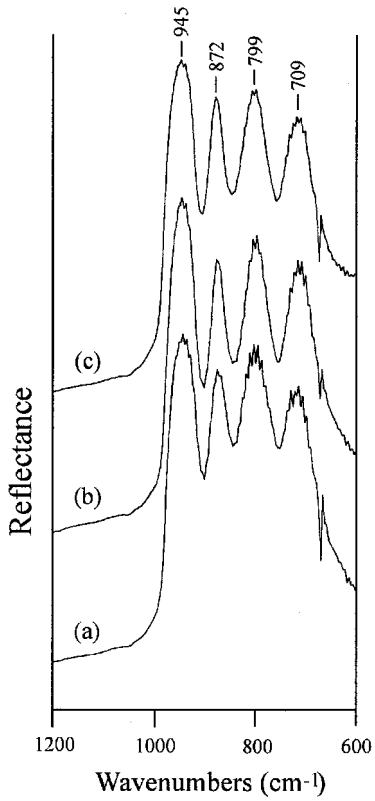

Fig. 7. DRIFT spectra collected at 550 °C following *in situ* calcination of the Ni-LTM precursors with a Ni/Mo ratio of (a) 0.75, (b) 1.0, and (c) 1.5.

spectra confirm that the phase present under reaction conditions is the β-phase, characterized by a tetrahedral coordination around the molybdenum atoms. These spectra also show that the local oxygen environment surrounding the molybdenum atoms is independent of the Ni/Mo ratio.

2. *Modeling the Defect Structure of Non-Stoichiometric Nickel Molybdates*

The high-temperature X-ray diffraction studies showed that the precursor phases having Ni/Mo ratios between 0.75 and 1.5 produced a single phase isostructural to β-$NiMoO_4$ upon calcination at 550 °C. This non-stoichiometric phase is proposed to have the general formula $Ni_{1+\delta}Mo_{1-\delta/3}O_4$, where δ represents the departure from stoichiometry and $-1/5 \leq \delta \leq 1/3$. This phase can be considered as a combination of the constituent binary oxides, NiO and MoO_3, where

$$Ni_{1+\delta}Mo_{1-\delta/3}O_4 = (1+\delta)NiO + (1-\delta/3)MoO_3 \tag{1}$$

To fully understand the behavior of the non-stoichiometric nickel molybdates, a knowledge of the defect chemistry of this ternary ionic crystal is required. In formulating the balance relationships and equilibria existing between various point defects, a basic assumption was made that the point defects could be treated thermodynamically as quasi-particles dissolved in the crystal [16]. It was further assumed that the point defects did not interact with each other.

In order to formulate an unambiguous set of disorder relationships and internal equilibria, the notation of Kröger and Vink [17] was used to represent defects as chemical species. Despite the structurally non-equivalent lattice positions for Ni and Mo in the structure of β-$NiMoO_4$ (Table 2), no differentiation of the sites was made when setting up the defect chemistry. In developing the defect chemistry relationships for the Ni-Mo-O system, the nickel and molybdenum atoms were initially considered to be in valence state of $+2$ and $+6$, respectively, and electronic disorder was initially assumed to be negligible. This analysis of the defect chemistry was therefore only valid at constant P_{O_2} and was used primarily as a tool to propose the majority point defects existing in the non-stoichiometric nickel molybdates.

2.1. *Balance relationships for ionic point defects in ternary molybdates.*

The non-stoichiometric nickel molybdate can be considered to be composed of its constituent binary oxides NiO and MoO_3 in a variable ratio. In general, if the Ni and Mo concentrations are allowed to vary independently of each other, the non-stoichiometric nickel molybdate can be considered in the form:

$$(1+\alpha)NiO \cdot (1+\beta)MoO_3 = Ni_{1+\alpha}Mo_{1+\beta}O_{4+\alpha+3\beta} \tag{2}$$

Defining w to be the difference between the fraction of oxygen vacancies and the fraction of interstitial oxygens,

$$w = V_O - O_i \tag{3}$$

the average number of oxygen anions in one-eighth of a unit cell is $4-w$, and by comparison to Eq. (2),

$$\alpha + 3\beta + w = 0 \tag{4}$$

The nickel molybdate can be characterized chemically by the ratio of the two constituent oxides:

$$(1+\beta)/(1+\alpha) \equiv 1+y \tag{5a}$$

Therefore, for small deviations from the ideal stoichiometric formula,

$$1+y \cong 1+\beta-\alpha \tag{5b}$$

Equations (5b) and (5a) define y as a measure of the deviation from the ideal stoichiometry. From Eqs. (4) and (5), it follows that

$$\alpha = -(3/4)y - (1/4)w \tag{6}$$

$$\text{and} \quad \beta = (1/4)y - (1/4)w \tag{7}$$

Using these relations, one can write balance equations for all the ions in the Ni-Mo-O system.

$$[Ni_{Ni}] + [Ni_{Mo}] + [Ni_i] = 1+\alpha = 1-(3/4)y-(1/4)w \tag{8}$$

$$[Mo_{Mo}] + [Mo_{Ni}] + [Mo_i] = 1+\beta = 1+(1/4)y-(1/4)w \tag{9}$$

$$[O_O] + [O_i] = 4+\alpha+3\beta = 4-w \tag{10}$$

A further set of balance equations can be obtained by summing up all the regular sites.

$$[Ni_{Ni}] + [Mo_{Ni}] + [V_{Ni}] = 1 \quad (11)$$

$$[Mo_{Mo}] + [Ni_{Mo}] + [V_{Mo}] = 1 \quad (12)$$

$$[O_O] + [V_O] = 4 \quad (13)$$

In deriving Eqs. (8) to (13), it has been assumed that the transition metal cations cannot be substituted for oxygen anions on their regular sites, and vice versa. Equations (8) to (13) can now be combined to obtain a set of equations involving only defect concentrations related to the deviation from the ideal stoichiometry:

$$[Mo_{Ni}] + [V_{Ni}] - [Ni_{Mo}] - [Ni_i] - (1/4)([V_O] - [O_i]) = (3/4)y \quad (14)$$

$$[Mo_{Ni}] - [V_{Mo}] - [Ni_{Mo}] + [Mo_i] + (1/4)([V_O] - [O_i]) = (1/4)y \quad (15)$$

$$[V_O] - [O_i] = w \quad (16)$$

Equations (14) to (16) can be used to catalog the possible combinations of ionic disorder with two different kinds of point defects, taking into account the condition of electrical neutrality for the overall crystal. Therefore, in Eqs. (8) to (13), only those combinations of defects that can occur which satisfy these equations with positive concentrations were considered for $y \cong 0$ (ideal stoichiometry), $y > 0$ (excess of MoO_3) and $y < 0$ (excess of NiO). The results are presented in Table 3.

If the concentration of oxygen defects is small in comparison to the concentration of cationic defects, then the possible combinations of defects reduce to those shown in Table 4. The ratio of concentrations of the two majority defects constituting a disorder type can be obtained by applying the condition of electrical neutrality, as shown in Table 4.

2.2. The defect structure of non-stoichiometric nickel molybdate. According to Eqs. (14) to (16), the deviation from ideal stoichiometry is always proportional to the concentrations of the majority point defects of the corresponding disorder type. If $y < 0$, corresponding to an excess of NiO, the nickel molybdate exists with a net excess of cations. As can be seen in the catalyst formulae of Table 1, $(N_{Ni} + N_{Mo}) / 2 > 1$ for Ni/Mo > 1, where N_i is the number of cations of type *i*. Based on the defect concentration relations shown in Table 4, it is proposed that the non-stoichiometric nickel molybdates having a Ni/Mo ratio greater than one have interstitial Ni atoms as the major defects that are compensated for by the presence of Mo vacancies.

If $y > 0$, corresponding to an excess of MoO_3, the nickel molybdate exists with a net deficiency of cations. As can be seen in the catalyst formulae of Table 1, $(N_{Ni} + N_{Mo})/2 < 1$ for Ni/Mo < 1. Based on the defect concentration relations presented in Table 4, it is proposed that the non-stoichiometric nickel molybdates having a Ni/Mo ratio less than one have Ni vacancies as the major defects that are compensated for by either interstitial Mo atoms, or Mo atoms occupying Ni sites. A Mo atom occupying a Ni site, however, would be in octahedral coordination (as in the α phase) and should show the corresponding IR absorptions. The DRIFT studies have shown an equivalence in the oxygen environment surrounding

Table 3. Ionic disorder types with two different kinds of point defects

Defect	$Ni_i^{\cdot\cdot}$	$Mo_i^{\cdot\cdot\cdot\cdot\cdot}$	V_{Ni}''	V_{Mo}''''''	Ni_{Mo}''''	$Mo_{Ni}^{\cdot\cdot\cdot\cdot}$	$V_O^{\cdot\cdot}$	O_i''
$Ni_i^{\cdot\cdot}$			$y \cong 0$	$y < 0$	$y < 0$			$y < 0$
$Mo_i^{\cdot\cdot\cdot\cdot\cdot}$			$y > 0$	$y \cong 0$	$y < 0$			$y > 0$
V_{Ni}''	$y \cong 0$	$y > 0$				$y > 0$	$y > 0$	
V_{Mo}''''''	$y < 0$	$y \cong 0$				$y > 0$	$y < 0$	
Ni_{Mo}''''	$y < 0$	$y < 0$				$y \cong 0$	$y < 0$	
$Mo_{Ni}^{\cdot\cdot\cdot\cdot}$			$y > 0$	$y > 0$	$y \cong 0$			$y > 0$
$V_O^{\cdot\cdot}$			$y > 0$	$y < 0$	$y < 0$			$y \cong 0$
O_i''	$y < 0$	$y > 0$				$y > 0$	$y \cong 0$	

Table 4. Defect concentration relations for cationic disorder types in nickel molybdates

$y < 0$	$[Ni_i^{\cdot\cdot}] = 3\,[V_{Mo}'''''']$	$[Ni_i^{\cdot\cdot}] = 2\,[Ni_{Mo}'''']$	$3\,[Mo_i^{\cdot\cdot\cdot\cdot\cdot}] = 2\,[Ni_{Mo}'''']$
$y \cong 0$	$[Mo_i^{\cdot\cdot\cdot\cdot\cdot}] = [V_{Mo}'''''']$	$[Mo_{Ni}^{\cdot\cdot\cdot\cdot}] = [Ni_{Mo}'''']$	$[Ni_i^{\cdot\cdot}] = [V_{Ni}'']$
$y > 0$	$3\,[Mo_i^{\cdot\cdot\cdot\cdot\cdot}] = [V_{Ni}'']$	$2\,[Mo_{Ni}^{\cdot\cdot\cdot\cdot}] = [V_{Ni}'']$	$2\,[Mo_{Ni}^{\cdot\cdot\cdot\cdot}] = 3\,[V_{Mo}'''''']$

the Mo, suggesting that only interstitial Mo atoms exist to compensate for the Ni vacancies.

3. Electronic Properties of Non-Stoichiometric Nickel Molybdates

The modeling of the defect chemistry of the series of non-stoichiometric nickel molybdates served only to suggest the possible identity of the majority point defects in nickel molybdates isostructural to β-$NiMoO_4$ that have Ni/Mo ratios varying between 0.75 and 1.5. Two of the key assumptions made in the modeling were constant valency of the transition metal cations and negligible electronic disorder. However, in addition to the intrinsic atomic disorder, extrinsic atomic disorder exists as a result of variable valency of the cations, and as a result of further adjustments in the stoichiometry due to variations in the partial pressure of one of the crystal components in the surrounding atmosphere. These variations are small relative to the ionic disorder, and concentrations of electrons and electron holes could therefore be disregarded in setting up the balance equations. However, when analyzing the electronic properties of these systems, the electronic defects make an essential contribution to the electrical conduction because the mobilities of the electronic defects are, in general, several orders of magnitude greater than those of interstitial ions or vacancies.

3.1. Experimental results of conductivity measurements. All the experimental data collected in the conductivity study on non-stoichiometric nickel molybdates were in the form of single arcs, centered slightly below the *x*-axis. The impedance data for a typical conductivity analysis are shown in Fig. 8. These data were collected on a sample of $Ni_{0.903}Mo_{1.032}O_4$ at 587 °C in 1 kPa of O_2. A semicircle was fitted to these data such that R could be calculated to be $1.3190 \times 10^8 \Omega$. The conductivity of this sample under these conditions could then be determined to be $\sigma = 8.82 \times 10^{-8}\,S.cm^{-1}$. In this manner, the conductivity was determined for each of the non-stoichiometric nickel molybdates listed in Table 1 as a function of both temperature and oxygen partial pressure.

The conductivity data for each of the nickel molybdates tested were found to be functions of both temperature and P_{O_2}. As an example, the conductivity of the nickel molybdate having a Ni/Mo ratio of 0.75 is shown in Fig. 9, where $\log(\sigma)$ is plotted as a function of the reciprocal temperature for two different O_2 partial pressures. As expected, the conductivity follows an Arrhenius type behavior, with an increase in conductivity with increasing temperature.

The most important determination in the conductivity studies is the dependence of the conductivity on the partial pressure of oxygen. The composition of the nickel molybdate will change by the addition or removal of oxygen from the structure until an equilibrium is reached between the structure and its surrounding atmosphere. Figure 10 shows the dependence of the conductivity on the O_2 partial pressure at 575 °C for the nickel molybdates having Ni/Mo ratios of 0.75, 1.0, and 1.5. As can be seen from Fig. 10, these three materials have very different dependencies on the partial pressure of O_2. At the lowest Ni/Mo

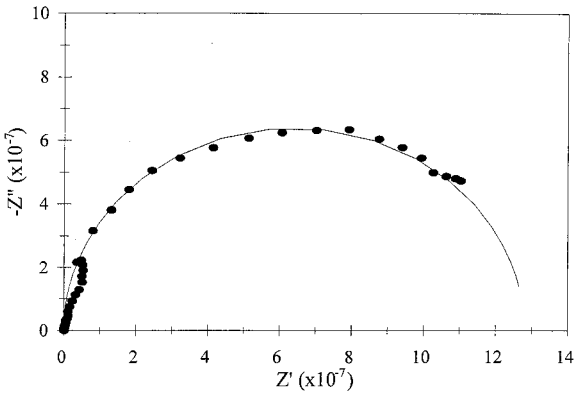

Fig. 8. Impedance data for $Ni_{0.903}Mo_{1.032}O_4$ at 587 °C in 1 kPa of O_2.

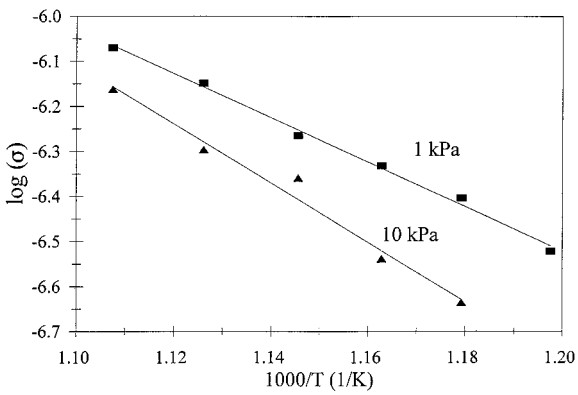

Fig. 9. Conductivity ($S.cm^{-1}$) of $Ni_{0.8}Mo_{1.067}O_4$ in 1 kPa and 10 kPa of O_2, displaying Arrhenius-type behavior.

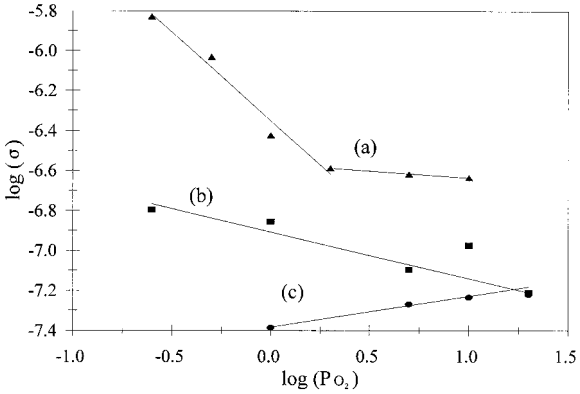

Fig. 10. Dependence of conductivity ($S.cm^{-1}$) on oxygen partial pressure (kPa) for materials with Ni/Mo ratios of (a) 0.75, (b) 1.0, and (c) 1.5.

ratio of 0.75, the conductivity decreases with increasing P_{O_2} due to oxygen up-take, thereby engaging otherwise free carriers. At a $P_{O_2} = 2$ kPa, there is a change in the downward slope of the graph to a slope that is almost zero, suggesting that the maximum oxygen uptake has been reached, and that a possible change in the charge carrier has occurred. The stoichiometric $NiMoO_4$ also shows a decrease in the conductivity with increasing P_{O_2}, a trend that was constant over the 0.25 kPa to 20 kPa range investigated. Linear regression of the conductivity data for this material showed the slope to be $-1/4.3$, suggesting a theoretical value of $-1/4$ or $-1/6$ that would indicate specific electronic defect chemistry. The conductivity of the stoichiometric $NiMoO_4$ is considerably smaller than that of the Ni-lean molybdate. Figure 10 shows, however, that the dependence of the conductivity on the O_2 partial pressure of the Ni-rich molybdate is completely opposite to the trends noted for the stoichiometric and Ni-lean molybdates. The conductivity of the material with a Ni/Mo ratio of 1.5 increases with increasing P_{O_2}. Linear regression of the conductivity data for this material showed the slope to be $+1/6.5$, a value fairly close to a theoretical $+1/6$ value. At a $P_{O_2} < 10$ kPa, the conductivity decreases in the order Ni/Mo = 0.75 > Ni/Mo = 1 > Ni/Mo = 1.5.

3.2. Correlation of conductivity data with defect structure of $Ni_{1+\delta}Mo_{1-\delta/3}O_4$. If the Ni/Mo ratio is greater than one, corresponding to an excess of NiO, the nickel molybdate exists with a net excess of cations. Based on the defect concentration relations shown in Table 4, it is proposed that these non-stoichiometric nickel molybdates have interstitial Ni atoms as the major defects that are compensated for by the presence of Mo vacancies. Given this excess of Ni atoms, it is proposed that the majority carrier arises from the oxidation of Ni^{2+} to Ni^{3+}, represented by the equation

$$2Ni_{Ni} + \frac{1}{2}O_2(g) + V_{Ni}^{x} + V_O^{x} \Leftrightarrow 2Ni_{Ni}^{\bullet} + O_O + V_{Ni}'' \tag{17}$$

From a chemical point of view, Eq. (17) can be considered as a representation of a solid solution of Ni_2O_3 in the NiO sublattice, that is, $Ni_2^{3+}V_{Ni}O_3$ replacing Ni_3O_3. For each Ni^{2+} vacancy, the charge must be compensated for by the oxidation of two Ni^{2+} ions to Ni^{3+}. Conduction occurring by transfer of an electron between Ni^{2+} and Ni^{3+} can be described as motion of holes in the valence band, making Eq. (17) equivalent to

$$\frac{1}{2}O_2(g) \Leftrightarrow O_O + V_M'' + 2h^{\cdot} \tag{18}$$

If this is indeed the dominant mechanism, analysis of the mass-action equilibrium constant shows, using the neutrality relation $2[V_M''] = [h^{\cdot}]$, that

$$[h^{\cdot}] \propto P_{O_2}^{+(1/6)} \tag{19}$$

and a plot of $\log(\sigma)$ against $\log(P_{O_2})$ should have a slope of $+1/6$. As shown in Fig. 10, the nickel molybdate having a Ni/Mo ratio of 1.5 does show a conductivity dependence on P_{O_2} very close to $+1/6$.

If the Ni/Mo ratio is less than one, corresponding to an excess of MoO_3, the nickel molybdate exists with a net deficiency of cations. Based on the defect concentration relations presented in Table 4, it is proposed that these non-stoichiometric nickel molybdates have Ni vacancies as the major defects that are compensated for by interstitial Mo atoms. Given this excess of Mo atoms, it is proposed that the majority carrier arises from the reduction of Mo^{6+} to Mo^{5+}, represented by the equation

$$2Mo_{Mo} + O_O \Leftrightarrow \frac{1}{2}O_2(g) + V_O^{\cdot\cdot} + 2Mo_{Mo}' \tag{20}$$

which, assuming Mo^{5+} to be equivalent to a quasi-free electron mobile in the conduction band at high temperatures, reduces to

$$O_O \Leftrightarrow \frac{1}{2}O_2(g) + V_O^{\cdot\cdot} + 2e' \tag{21}$$

If this is indeed the dominant mechanism, analysis of the mass-action equilibrium constant shows, using the neutrality relation $2[\mathrm{V_O^{\cdot\cdot}}] = [\mathrm{e'}]$, that

$$[e'] \propto P_{O_2}^{-(1/6)} \tag{22}$$

and a plot of $\log(\sigma)$ against $\log(P_{\mathrm{O_2}})$ should have a slope of $-1/6$. As shown in Fig. 10, the nickel molybdate having a Ni/Mo ratio of one shows a conductivity dependence on $(P_{\mathrm{O_2}})$ only slightly larger than $-1/6$. The conductivity dependence of the most Ni-lean molybdate shows a much stronger dependence on the partial pressure of oxygen, suggesting that Eq. (20) is not the only reaction taking place. Electron generation may be enhanced by possible ionization of the nickel vacancies, giving a dependence of the conductivity on the oxygen partial pressure that deviates from that derived if Eq. (20) was the dominant charge carrier generation mechanism.

Conclusions

The conductivity studies have clearly demonstrated that the conductivity of the non-stoichiometric nickel molybdates is a strong function of the defect chemistry of these materials. Analysis of the defect chemistry of these materials allowed for a suggestion of the majority point defects for nickel molybdates having both high and low Ni/Mo ratios. Structural characterization of the non-stoichiometric nickel molybdates resulting from calcination of the Ni-LTM precursors covering the full range of Ni/Mo ratios has shown them to be single phase and isostructural to β-$\mathrm{NiMoO_4}$. Given this equivalence in physical structure, a determination of the differences in the electronic properties of these materials has provided a basis for the correlation of the catalytic properties of these Ni-Mo-O systems with their defect structures.

Acknowledgments

This work was supported by the National Science Foundation (CTS-9257223 and DMR-9400334). The authors would like to thank Peter Kloumann of MIT's CMSE for assistance with the high-temperature diffraction studies. The assistance of Ruma Chakravorty in setting up the ac impedance spectrometer is greatly appreciated.

References

1. F. Cavani and F. Trifirò, *Catalysis Today*, **24**, 307 (1995).
2. C. Mazzocchia, C. Aboumrad, C. Diagne, E. Tempesti, J.M. Herrmann, and G. Thomas, *Catal. Lett.*, **10**, 181 (1991).
3. C. Mazzocchia, R. Anouchinsky, A. Kaddouri, M. Sautel, and G. Thomas, *J. Therm. Anal.*, **40**, 1253 (1993).
4. C. Mazzocchia, A. Kaddouri, R. Anouchinsky, M. Sautel, and G. Thomas, *Solid State Ionics*, **63**, 731 (1993).
5. G. Minow, K. Schnabel, and G. Ohlmann, *React. Kinet. Catal. Lett.*, **22**, 389 (1983).
6. C. Mazzocchia, F. Di Renzo, C. Aboumrad, and G. Thomas, *Solid State Ionics*, **32**, 228 (1989).
7. R.M. Martin-Aranda, M.F. Portela, L.M. Madeira, F. Freire, and M. Oliveira, *Appl. Catal. A*, **127**, 201 (1995).
8. D. Levin and J.Y. Ying, submitted to *J. Catal.*
9. D. Levin, S.L. Soled, and J.Y. Ying, *Chem. Mater.*, **8**, 836 (1996).
10. D. Levin, S.L. Soled, and J.Y. Ying, *Inorg. Chem.*, **35**, 4191 (1996).
11. GSAS, General Structure Analysis System, A.C. Larson and R.B. von Dreele, LANSCE, Los Alamos National Laboratory, copyright 1985–1994 by the Regents of the University of California.
12. S.C. Abrahams and J.M. Reddy, *J. Chem. Phys.*, **43**, 2533 (1965).
13. A.W. Sleight and B.L. Chamberland, *Inorg. Chem.*, **7**, 1672 (1968).
14. P. Thompson, D.E. Cox, and J.B. Hastings, *J. Appl. Cryst.*, **20**, 79 (1987).
15. S. Sheik Saleem, G. Aruldhas, and H.D. Bist, *J. Solid State Chem.*, **48**, 77 (1983).
16. H. Schmalzried, *Progress in Solid State Chemistry*, **2**, 265 (1965).
17. F.A. Kröger and H.J. Vink, *Solid State Phys.*, **3**, 307 (1956).